Anomalous temperature behavior of the chiral spin helix in $CrNb_3S_6$ thin lamellae

Y. Togawa[1,2], J. Kishine[3], P. A. Nosov[4,5], T. Koyama[6], G. W. Paterson[2],
S. McVitie[2], Y. Kousaka[7], J. Akimitsu[7], M. Ogata[8], A. S. Ovchinnikov[9,10]

[1]*Department of Physics and Electronics, Osaka Prefecture University, 1-1 Gakuencho, Sakai, Osaka 599-8531, Japan*
[2]*School of Physics and Astronomy, University of Glasgow, Glasgow, G12 8QQ United Kingdom*
[3]*Division of Natural and Environmental Sciences,*
The Open University of Japan, Chiba, 261-8586, Japan
[4]*Department of Physics, St. Petersburg State University, St. Petersburg 198504, Russia*
[5]*NRC Kurchatov Institute, Petersburg Nuclear Physics Institute, Gatchina 188300, Russia*
[6]*Department of Materials Science, Osaka Prefecture University, 1-1 Gakuencho, Sakai, Osaka 599-8531, Japan*
[7]*Research Institute for Interdisciplinary Science, Okayama University, Okayama, Okayama, 700-8530, Japan*
[8]*Department of Physics, the University of Tokyo, Hongo, Bunkyo, Tokyo 113-0033, Japan*
[9]*Institute of Natural Sciences and Mathematics, Ural Federal University, Ekaterinburg, 620083, Russia and*
[10]*Institute for Metal Physics, Ural Division of RAS, Ekaterinburg 620137, Russia*

Using Lorentz transmission electron microscopy and small-angle electron scattering techniques, we investigate the temperature-dependent evolution of a magnetic stripe pattern period in thin-film lamellae of the prototype monoaxial chiral helimagnet $CrNb_3S_6$. The sinusoidal stripe pattern appears due to formation of a chiral helimagnetic order (CHM) in this material. We found that as the temperature increases, the CHM period is initially independent of temperature and then starts to shrink above the temperature of about 90 K, which is far below the magnetic phase transition temperature for the bulk material, T_c (123 K). The stripe order disappears at around 140 K, far above T_c. We argue that this cascade of transitions reflects a three-stage hierarchical behavior of melting in two dimensions.

Introduction. Stripe pattern formation is found in a wide variety of ordered systems with many degrees of freedom. It has been of considerable interest and intensively discussed in condensed matter physics, including the areas of density waves [1–3], Wigner crystals [4], magnetic domains [5], superconductors [6], and liquid crystals [7, 8].

Temperature evolution of the stripe pattern is one of the fundamental and intriguing issues in this research area. Chiral helimagnets with the chiral helical order, being stabilized by an antisymmetric exchange interaction [9, 10], exhibit robust and stable phase coherence on a macroscopic length scale [11]. Because of this feature, purely sinusoidal phase modulation is realized in this class of materials [12, 13]. The regularity of the magnetic order makes chiral helimagnets a promising candidate system to carry out accurate determination of the spatial period and wave number of the stripe magnetic pattern.

In this Letter, we report experimental analyses of the periodicity of a chiral helimagnetic order (CHM) in thin-film lamellae of a monoaxial chiral helimagnet $CrNb_3S_6$ in a wide temperature range by using Lorentz transmission electron microscopy and small-angle electron scattering (SAES) techniques. From direct visualization of the spin helix order, we found three stages in the temperature, T, evolution of the CHM period. First, the CHM keeps its period constant at low T. As T increases, a shrinkage of the period occurs at around 90 K, followed by a linear dependence of the wave number on T, which is far below the magnetic phase transition temperature for the bulk crystal, T_c, of 123 K. In the end, the stripe

order vanishes above 140 K. The appearance of these two characteristic temperatures is hardly explained through mean-field theory of three dimensional (3-D) phase transitions. Remarkably, the observed temperature evolution of the CHM pitch is in line with predictions of the theory of melting in two dimensions [14]. Specifically, one may identify the experimental results just described as a low temperature solid phase, a floating solid phase at intermediate temperatures, and an isotropic fluid phase at higher temperatures. This process has not previously been considered for the chiral helimagnetic system and we believe our results represent the observation of two dimensional (2-D) melting in a magnetic system.

Experiment. Single crystals of transition-metal dichalcogenide $CrNb_3S_6$ were grown using a chemical-vapor transport method, as described elsewhere [15]. $CrNb_3S_6$ has a hexagonal crystalline structure belonging to the space group $P6_322$ and thus exhibits an antisymmetric Dzyaloshinskii-Moriya (DM) exchange interaction [9, 10] which competes with a symmetric Heisenberg exchange interaction. As a consequence, the CHM appears with a harmonic spatial modulation and a fixed sense of rotation of the magnetic moment about the principal (c) axis of the crystal, corresponding to the helical axis, as depicted in Fig. 1(a).

The magnetic-field dependence of the CHM period at a constant temperature is well understood: the CHM transforms into a nonlinear helicoidal spin order, frequently called chiral spin soliton lattice (CSL), in the presence of a magnetic field applied in a direction perpendicular to the helical axis of the CHM [11, 16]. The CSL changes its period with increasing field strength during
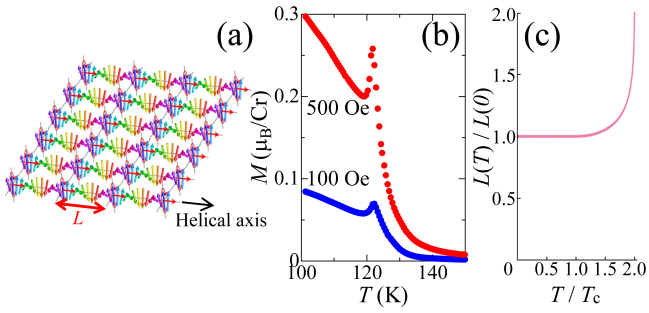
FIG. 1: (a) Schematic of the chiral helimagnetic order (CHM) with a period L. (b) Magnetization curves of the bulk $CrNb_3S_6$ single crystal as a function of T with a small H applied perpendicular to the helical axis.(c) Temperature dependence of L expected from 3-D mean field theory.

FIG. 2: Stripe pattern in a thin lamella of $CrNb_3S_6$ crystal at various temperatures. Lorentz Fresnel images and SAES data are given in (a) to (e) and (f) to (j), respectively. The insets in (a) to (c) present harmonic intensity profiles of the CHM. A pair of fundamental satellite peaks are indicated by arrows in (f) to (i). Intensity linetrace along dotted arrows in the c^* direction is shown below (i), indicating the presence of spots associated with the magnetic stripe pattern at 137 K.

the CSL formation, which allows the chiral spin system to present many striking physical responses [12, 13] such as discretized multi-valued magnetoresistance [17–19] and collective resonant dynamics sensitive to excitation polarization [20]. In contrast, in this Letter, we focus on the temperature dependence of the CHM period at small constant magnetic field.

Before preparing thin platelet specimens for Lorentz electron microscopy observations, a temperature dependence of the magnetization of the original bulk $CrNb_3S_6$ crystal was measured in order to examine the crystal quality. Figure 1(b) shows the temperature dependent magnetization curves for the bulk crystal. The data were taken at various magnetic fields in the configuration of H applied perpendicular to the helical c axis using a commercial superconducting quantum interference device magnetometer. A sharp peak of the magnetization appears and the peak position remains almost the same at small H. However, it moves toward lower T with further increasing H, as reported elsewhere [13, 17]. This behavior corresponds to the phase transition from the CHM (or CSL) phase into a paramagnetic one, which is well described by the 3-D mean field theory based on the chiral sine-Gordon model [21, 22]. This consistency supports the validity of the 3-D mean field picture for the bulk crystal.

Following a standard definition of the critical temperature T_c as the temperature giving the peak of the magnetization at small H, e.g., less than 100 Oe, T_c is determined to be 123 K for the bulk crystal used in this study. This value is smaller than the maximum value of 132 K, obtained in the bulk crystals synthesized in the laboratory. However, as seen in the following paragraphs, the CHM period is 48 nm at the lowest T used for this crystal. This value is consistent with that obtained in previous studies [23, 24], which guarantees that the present specimen has the same quality as those studied in the literature. Neutron scattering experiments [24]
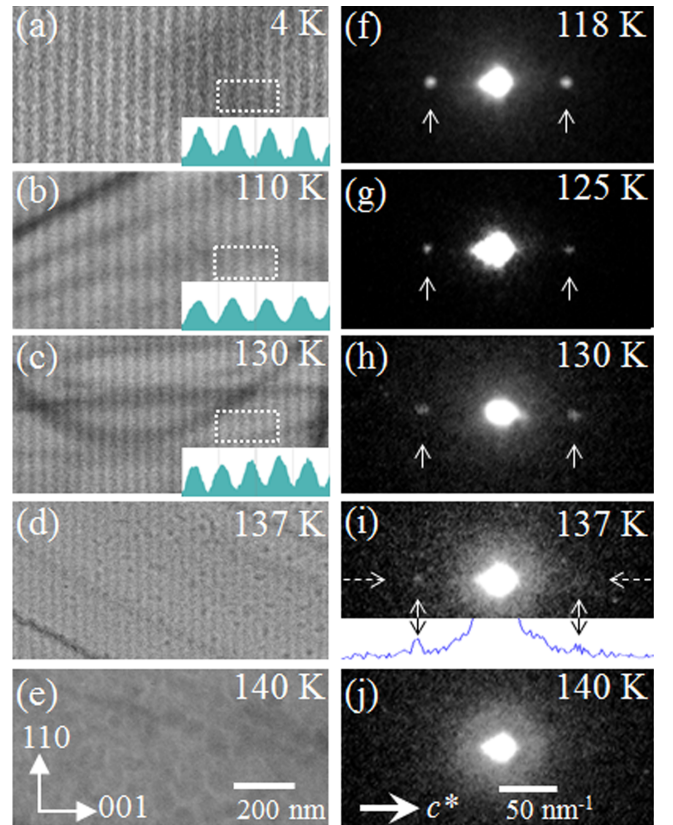
showed that the CHM wave number remains unchanged at 13 K and 100 K for the bulk crystal.

Thin (< 100 nm) platelet specimens for transmission electron microscopy (TEM) analyses were prepared from the bulk crystal using focused ion beam methods. TEM observations were performed in a nearly-H-free environment (with a residual $H \sim 100$ Oe) by operating the electron microscope without the electromagnetic objective lens being excited.

Real-space observations of magnetic structures were performed by means of the Fresnel mode of Lorentz microscopy [25] using model JEM-2010 or JEM-2100 transmission electron microscope with an acceleration voltage of 200 kV. Differential phase contrast (DPC) mode [26] was also adopted for precise evaluation of the stripe pattern period using a JEOL ARM-200CF scanning transmission electron microscope. In addition, SAES experiments [25] were performed to accurately determine the value of the wave number in reciprocal space. To exam-
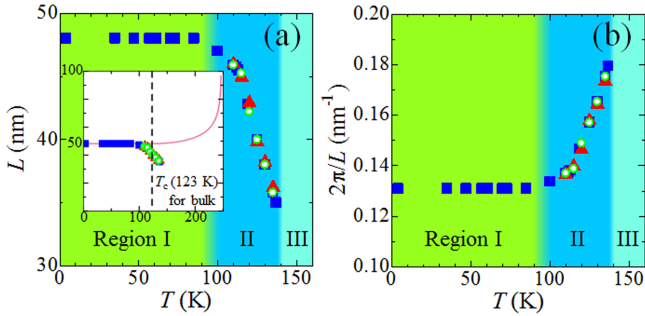
FIG. 3: The CHM period (a) and wave number (b) as a function of T in a thin lamella of CrNb$_3$S$_6$ crystal. Blue squares represent the data obtained by the Lorentz Fresnel and DPC methods. Green circle and red triangles correspond to the SAES data taken with increasing and decreasing T, respectively. The inset in (a) shows the curve derived from the 3-D mean field theory together with the experimental data and T_c for the bulk crystal. Three regions which show different kinds of T dependence are clearly seen. Regions I, II, and III correspond to the solid phase (the CHM with the constant period), the floating solid phase (the shrinkage of the CHM period), and the isotropic fluid phase (the paramagnetic regime), respectively.

ine the behavior in a temperature range above 100 K, TEM samples were cooled using a liquid N$_2$ holder. For performing Lorentz microscopy at lower temperatures for many hours, the samples were cooled down to below 2 K using superfluid He in the seventh generation cryogenic transmission electron microscope available in Nagoya University, Japan [27]. In this case, the specimen temperature was around 4 K, which is lower than temperatures achieved using a standard liquid He holder. The temperature dependence of the CHM period was measured with decreasing T below 100 K, while it was examined with cycling T above 100 K.

A series of Fresnel-mode Lorentz images and SAES data were taken at various temperatures as shown in Fig. 2. A stripe pattern was obtained in the real-space images and its intensity profile appears to be modulated in a harmonic manner, as highlighted in Figs. 2(a) to 2(c). The harmonic nature of the magnetic modulation was directly demonstrated in the SAES data, as presented in Figs. 2(f) to 2(j). A pair of spots were clearly observed only at a wave number of the first harmonic position at 110 K, as reported elsewhere [11]. These CHM spots remain present without any accompanying higher harmonics at 130 K, which is above the value of T_c for the original bulk crystal. However, no spots were observed at 140 K. One of the important findings is that the harmonic magnetic structure appears in a wide range of temperatures from 4 K to 137 K, indicating that the CHM survives even above T_c for the bulk crystal.

Figure 3 shows how the CHM period L and wave number Q vary with T. Precise measurements of L and Q

were performed in the real and reciprocal space by means of Lorentz Fresnel and DPC methods and SAES method, respectively. The temperature dependences of L and Q are consistent with each other and thus the relationship of $Q = 2\pi/L$ hold as expected. It is clear that the CHM keeps its period constant up to about 90 K, at around which temperature it starts to decrease with further increasing T, e.g., a small drop of the period is found at 100 K. Then, the stripe contrast suddenly disappears above 137 K. Interestingly, the CHM period and wave number show a linear dependence on T above 110 K and grows until the temperature reaches 137 K, as clearly seen in Figs. 3(a) and 3(b), respectively. The linear dependence can be found in both cases since the amount of changes are smaller than the values of L and Q at the lowest temperature. Importantly, the observed behavior is inconsistent with that expected for the 3-D mean field theory drawn in Fig. 1(c) and the inset of Fig. 3(a). Moreoever, Lorentz microscopy observations reveal three T regions (regions I, II and III) based on the temperature dependence of the CHM period and wave number, as indicated in Fig. 3.

Theoretical support. The temperature dependence of the magnetization shown in Fig. 1(b) indicates that the 3-D mean field picture works well in the bulk sample [21, 22]. First, we demonstrate the temperature dependence of the CHM and CSL periods based on this picture. The CSL period is given by a formula $L = 8K(\kappa)E(\kappa)/(\pi q_0)$ [12, 16], where $K(\kappa)$ and $E(\kappa)$ respectively denote the elliptic integrals of the first and second kinds with the elliptic modulus κ ($0 \leq \kappa \leq 1$). The modulus κ is determined by minimizing the CSL formation energy and determined through the relation $\kappa/E(\kappa) = \sqrt{H/H_c}\sqrt{m(H,T)/m(H,0)}$ where H_c is the critical field at the zero temperature and $m(H,T)$ is the field and temperature dependent amplitude of the magnetic moment which is determined by minimizing the mean field free energy density[21], $f = (T/T_c - 1)m^2 + bm^4 - mH$, where b is a temperature-independent positive constant. Then, at the constant field, the temperature dependent modulus κ gives the temperature dependence of L, which is presented in Fig. 1(c). In the the 3-D mean field picture, L hardly increases upon increasing T below T_c and starts to rapidly increase far above T_c. A similar divergent behavior of L is also reported in the recent study [28].

In the experimental findings mentioned above, the linear temperature-dependence of the wave number in the temperature region II seems to be a challenging issue, since this result goes against the 3-D mean eld theory as evident from Fig. 1(c). We will argue that this feature might be explained within the theory of 2-D melting [14].

Prior to substantiaing this claim based on the 2-D model, we first note that Lorentz microscopy and SAES experiments [11, 25] enable us to monitor the spatial distribution of the magnetic moment associated with the CHM, $\boldsymbol{M}(\boldsymbol{r}) = M_0 [\hat{\boldsymbol{e}}_x \cos\varphi(\boldsymbol{r}) \pm \hat{\boldsymbol{e}}_y \sin\varphi(\boldsymbol{r})]$, where

the xy plane corresponds to the crystallographic ab plane and the helical z axis coincides with the crystallographic c axis. The sign defines the chirality of the helix. The amplitude of the order parameter M_0 is the value of the magnetic moment and the phase $\varphi(\boldsymbol{r})$ describes the spatial modulation of the CHM structure. In real-space images, the CHM is visualized as a modulated stripe pattern of an in-plane component of the magnetic moment. As complementary information provided by SAES, the harmonically-modulated CHM is detected as a pair of fundamental satellite peaks in the reciprocal k space.

To describe the temperature evolution of the stripe pattern, we begin with the 2-D classical phase Hamiltonian of the Pokrovsky-Talapov model [29, 30], which has been discussed in the context of CHM [31, 32],

$$H = \int dx dz \left[\frac{\sigma}{2} \left(\partial_z \varphi - \delta \right)^2 + \frac{\nu}{2} \left(\partial_x \varphi \right)^2 + \lambda \cos \varphi \right], \quad (1)$$

where the spin stiffness parameters, σ and ν ($\sigma \ll \nu$), originate from the anisotropic ferromagnetic exchange interactions within the xz plane, the misfit parameter δ stems from the antisymmetric exchange interaction, and the pinning potential λ comes from the Zeeman coupling with the small external magnetic field applied perpendicular to the helical axis.

Depending on temperature ranges, the starting Hamiltonian (1) is mapped onto different effective models. In the low temperature regime (regime I), the fermionic representation is valid, as demonstrated by Schulz [33]. In the intermediate and high temperature regimes (regimes II and III, respectively), the renormalization-group (RG) scheme works well [34, 35]. The whole sequence of the analysis is consistent with a universal hierarchy of 2-D melting phenomena proposed by Nelson and Halperin [14].

In this general scheme, a regular solid state undergoes a transition into a floating solid phase with an orientational order followed by an isotropic fluid phase upon increasing temperature [14]. In our experiment on chiral helimagnets, the solid phase corresponds to the CHM one with a constant period, the floating solid phase is indicated by the shrinkage of the CHM period, and the isotropic fluid phase arises as the paramagnetic phase.

To specify the correspondence, we discuss the theoretical scheme in more detail. The fermionic model by Schulz is introduced by applying the transfer integral technique to the Hamiltonian (1) which maps it firstly onto the $(1+1)$ quantum bosonic Hamiltonian, where the space coordinate lies along the z-axis. This bosonic Hamiltonian is then transformed into the fermionic Tomonaga-Luttinger model with the umklapp scattering term originating from the Zeeman coupling term, $\lambda \cos \varphi$. The misfit parameter δ plays a role of the chemical potential of the fermion system.

In the fermion model framework, the umklapp processes cause the Mott insulating phase with a gap be-

tween the lower Hubbard band (LHB) and the upper one (UHB) [33]. As a consequence, the phase coherence of the pattern is protected by the Mott gap, where the chemical potential lies inside the gap. An appearance of additional kinks corresponds to thermally excited fermions in the UHB, which is interpreted as a starting of the melting. As has been demonstrated by Schulz, the orientational phase order just above the melting point is supported by the strongly anisotropic nature of spatial correlations.

The intermediate temperature regime may be treated by the RG theory of the floating devil's staircase in two dimensions [35]. According to this approach, the initial Hamiltonian (1) may be considered as a grand-canonical ensemble with a chemical potential, μ, coupled with the kink density, ρ. A key insight of the formalism is that the phase fluctuations undergo the RG transformations after the periodic background is subtracted. It was demonstrated that the RG flows belong to the Kosteritz-Thouless (KT) universality class, but, in contrast to the original KT theory, they rapidly terminate in our system due to the presence of sharp cut-off functions which reflect the existence of the natural length scale related with a distance between kinks [35]. Just above the melting transition, the RG trajectories flow towards the regime where the Mott gap collapses with the chemical potential μ being fixed. Therefore, possible excitations may be regarded as proliferation of the fermions into the UHB. In other words, as T increases, new kinks enter into the system following a linear dependence of the kink density on temperature, $\rho \propto \mu T + f(\mu)$, where $f(\mu)$ is a function of only the chemical potential [35]. This linearly temperature dependent kink density is consistent with the experimentally observed linear dependence of the wave number above 110 K.

At the final stage, the stripe order disappears and is followed by a high-temperature paramagnetic phase. As discussed previously by some of the authors, the initial Hamiltonian (1) may be reformulated in terms of the massive Thirring model, where it was argued that the misfit parameter rules out a KT transition, because it acts as an effective in-plane electric field that prevents a formation of bound vortex-antivortex pairs [34].

Concluding remark. In this Letter, we examined the temperature-dependent evolution of a magnetic stripe pattern associated with the harmonic CHM in thin lamellae of $CrNb_3S_6$ using Lorentz electron microscopy and SAES techniques. A notable feature found in these measurements is the shrinkage of the CHM period above $T \sim 90$ K, far below the magnetic phase transition temperature for the bulk material. We argued that this temperature dependence reflects the universal behavior intrinsic to 2-D melting [14]. This observation might be regarded as manifestation of Halperin-Nelson hierarchy of the melting process in a magnetic system. We believe that the present work will gain insight on the hierarchy of 2-D melting and shed light on the physics of patterns

in a magnetic system.

---

[1] G. Grüner, Rev. Mod. Phys. **60**, 1129 (1988).

[2] G. Grüner, Rev. Mod. Phys. **66**, 1 (1994).

[3] A. Bianconi and N. L. Saini, (eds.), *Stripes and Related Phenomena,* (Springer US, Boston, 2000).

[4] L. Rademaker, Y. Pramudya, J. Zaanen, and V. Dobrosavljević, Phys. Rev. E **88**, 032121 (2013).

[5] A. Hubert and R. Schäfer, *Magnetic Domains: the Analysis of Magnetic Microstructures*, (Springer-Verlag, Berlin, Heidelberg, 1998).

[6] S. A. Kivelson, I. P. Bindloss, E. Fradkin, V. Oganesyan, J. M. Tranquada, A. Kapitulnik, and C. Howald, Rev. Mod. Phys. **75**, 1201 (2003).

[7] P.-G. De Gennes, Solid State Commun. **6**, 163 (1968).

[8] S. Chandrasekhar, *Liquid crystals*, (2nd edition, Cambridge University Press, 1992).

[9] I. E. Dzyaloshinskii, J. Phys. Chem. Solids **4**, 241 (1958).

[10] T. Moriya, Phys. Rev. **120**, 91 (1960).

[11] Y. Togawa *et al.*, Phys. Rev. Lett. **108**, 107202 (2012).

[12] J. Kishine and A. S. Ovchinnikov, Solid State Physics **66**, 1 (2015).

[13] Y. Togawa, Y. Kousaka, K. Inoue, and J. Kishine, J. Phys. Soc. Jpn. **85**, 112001 (2016).

[14] B. I. Halperin and D. R. Nelson, Phys. Rev. Lett. **41**, 121 (1978).

[15] Y. Kousaka *et al.*, Phys. Res., Sect. A **600**, 250-253 (2009).

[16] I. E. Dzyaloshinskii, Sov. Phys. JETP **20**, 665 (1965).

[17] Y. Togawa *et al.*, Phys. Rev. Lett. **111**, 197204 (2013).

[18] Y. Togawa *et al.*, Phys. Rev. B **92**, 220412 (2015).

[19] L. Wang *et al.*, Phys. Rev. Lett. **118**, 257203 (2017).

[20] F. J. T. Goncalves *et al.*, Phys. Rev. B **95**, 104415 (2017).

[21] J. Kishine, K. Inoue and K. Kikuchi, J. Mag. Mag. Mat. **310**, 1386 (2007).

[22] M. Shinozaki, S. Hoshino, Y. Masaki, J. Kishine, and Y. Kato, J. Phys. Soc. Jpn. 85, 074710 (2016).

[23] T. Moriya and T. Miyadai, Solid State Commun. **42**, 209 (1982).

[24] T. Miyadai *et al.*, J. Phys. Soc. Jpn. **52**, 1394 (1983).

[25] Y. Togawa, Microscopy **62** (Suppl. 1), S75 (2013).

[26] S. McVitie *et al.*, Ultramicroscopy, **152**, 57 (2015).

[27] Y. Fujiyoshi, Protein Sci. **20**, 806817 (2011).

[28] V. Laliena, Y. Kato, G. Albalate, and J. Campo, arXiv:1804.10039.

[29] V. L. Pokrovsky and A. L. Talapov, Phys. Rev. Lett. **42**, 65 (1979).

[30] V. L. Pokrovsky and A. L. Talapov, Zh. Eksp. Teor. Fiz. **78**, 269 (1980) [Sov. Phys. JETP **51**, 134 (1980)].

[31] J. Heurich, J. König, and A. H. MacDonald, Phys. Rev. B **68**, 064406 (2003).

[32] J. Kishine, I. G. Bostrem, A. S. Ovchinnikov, and Vl. E. Sinitsyn, Phys. Rev. B **59**, 014419 (2014).

[33] H. J. Schulz, Phys. Rev. B **22**, 5274 (1980).

[34] P. A. Nosov, J. Kishine, A. S. Ovchinnikov, and I. Proskurin, Phys. Rev. B 96, 235126 (2017).

[35] B. Horovitz, T. Bohr, J. M. Kosterlitz, and H. J. Schulz, Phys. Rev. B **28**, 6596 (1983).

[36] The DPC data used for Fig. 3 are available at: http://dx.doi.org/10.5525/gla.researchdata.701.